Seismic geomorphology of shallow-water lacustrine deltas in the Paleocene Huanghua Depression, Bohai Bay Basin, Eastern China

Jiahao Wang[1], Zhenliang Guan[1], Andrew D. La Croix[2], Qingkui Wang[3], Ling Ji[3], Jian Sun[3]

1. Key Laboratory of Tectonics and Petroleum Resources (China University of Geosciences), Ministry of Education, Wuhan, Hubei 430074, China;

2. Earth Sciences, University of Waikato, Hamilton 3240, New Zealand;

3. No.3 Oil Production Factory, Dagang Oil-field Branch Company, CNPC, Cangzhou, 061000, China

Corresponding author: telephone number: +86-27-67883067, email address: cugwangjiahao@163.com

Abstract: The most important sedimentary facies comprising shallow-water lacustrine deltas are distributary channels, and these form abundant ribbon-shaped sand bodies that are excellent petroleum reservoirs. However, distributary channel sandstones are notoriously difficult to correlate and characterize in the subsurface based on well data alone. Here, we show how seismic geomorphology can be used to map lacustrine deltaic sedimentary successions in the First Member of the Kongdian Formation within the Zilaitun Oilfield, Huanghua Depression (China). Using core and wireline logs, this study identified distributary channels as the dominant sedimentary facies. Together with mottled grey-green or maroon mudstones and locally shingled progradational seismic reflection architecture, this indicates that deltas were built in a weakly-oxidized shallow-water lacustrine environment. Next, core observations were linked to seismic data to produce a successive series of stratal slices and root mean square amplitude attribute (RMSAA) maps. The RMSAA maps allowed distributary channel, mouth bar, and beach bar facies to be identified and mapped across the study area. Two patterns of distributary channels emerged from the data: (1) a distributive pattern with a lower concentration of distributary channels; and, (2) an anastomosing deltaic pattern with a high concentration of bifurcated distributary channels. Based on the seismic geomorphological analysis we show that the succession records three phases of delta evolution - retrogradation, aggradation, and progradation - which

combine to form 3rd-order sequences. From a petroleum reservoir point of view, the distributive pattern yields narrower, thicker, and less connected sand bodies than the anastomosing pattern. This is consistent with observations from modern shallow-water lacustrine delta systems, providing independent support for the interpretation and highlighting the effectiveness of using seismic geomorphology.

Key words: Seismic geomorphology; Shallow-water lacustrine delta; Distributary channel; Seismic stratal slice; Root mean square attribute map.

1. Introduction

Shallow-water lacustrine deltas form above normal wave base at water depths generally less than ten meters and depositional gradients of less than 0.5° (Donaldson, 1974; Overeem et al., 2003; Olariu and Bhattacharya, 2006； Zou et al., 2008; Jin et al., 2014). Distributary channels are the dominant sedimentary facies comprising shallow-water lacustrine deltas, and are increasingly identified from lacustrine basins where they produce a number of dense striped sand bodies that are excellent petroleum reservoirs (Zou et al, 2008; Zhu et al., 2008; Li et al., 2009; Zhao et al., 2011; Wang et al., 2012; Jin et al., 2014; Zhu et al., 2017). There is, however, a difficulty in mapping distributary channel sand bodies using conventional well-based sedimentary facies analyses alone (i.e., sandstone isopach or percentage maps), due to the ambiguity of sand body connectedness between neighboring wells (Zeng et al., 2012). Thus, seismic geomorphological analysis provides an alternative way to map shallow-water lacustrine deltas and decrease uncertainty about reservoir connectivity.

Based on the correlation between seismic attribute maps and sedimentary facies distributions, seismic geomorphology was developed as a way to use seismic data to study sedimentary facies distributions and depositional processes (Posamentier, 2002; Posamentier and Kolla, 2003; Sylvester et al., 2012). Since then it has been successfully applied to investigate a variety of sedimentary systems such as shelf ridges (e.g. Posamentier, 2002; Posamentier and Wood, 2007), submarine fans (Kolla et al., 2001; Posamentier and Kolla, 2003), deltas (Dong et al., 2014), fluvial and tidal-fluvial

systems (Carter, 2003; Hubbard et al., 2011), and lacustrine beach bars (Zhao et al., 2014). It is particularly effective for mapping various types of channels such as fluvial channels, gravity flow channels in submarine fans, and distributary channels in deltas, as well as associated sedimentary elements such as abandoned channels, levees, overbanks, and crevasse-splays (Miall, 2002; Loucks, 2011; Zeng et al., 2012; 2013; Zhu et al., 2017). This makes it possible to acquire quantitative data such as channel width and sinuosity (Kolla et al., 2001; Posamentier and Kolla, 2003; Wood and Kristine, 2009; Sylvester et al., 2012). Nevertheless, few seismic geomorphological studies have mapped shallow-water lacustrine delta systems so far.

In this study, we undertake a seismic geomorphological analysis of the First Member of the Kongdian Formation, in the Zilaitun Oilfield, Huanghua Depression, aiming to map shallow-water lacustrine deltas (and especially their distributary channels) in detail.

2. Geological Setting

The Huanghua Depression, a continental rift lacustrine depression, is about 17,000 km^2 in area, and is located in the central Bohai Bay Basin of eastern China (Fig. 1A). In relation to back-arc extension induced by the West Pacific Plate's subduction under the Eurasian Plate, the depression experienced a Paleogene rift stage and a Neogene post-rift stage (Allen et al., 1997; Ren et al., 2002; Ye et al., 2013)., Controlled by northeast-strike normal faults during the rift stage, five tectonic belts -- Xuyangqiao-Helongcun, Kongdian, Nandagang, Beidagang, and Tanggu-Xinggang -- developed with horst or faulted roll-over anticline structural patterns. These are favorable petroleum accumulations, with more than ten million tons of oil discovered to date (Dong et al., 2014). Among them, the Kongdian belt, in which the Zilaitun Oilfield (40 km^2 in area) is located, occurs as a faulted roll-over anticline due to the combined effects of the Cangdong and Xuxi faults (Figs. 1B, C).

In the Zilaitun Oilfield, the Paleogene stratigraphy has been subdivided based on seismic interpretation and lithologic assemblages into 3 formations, 3 members, 6 sand-sets, and 17 intervals (Fig. 1C, Table 1). The three formations are the Paleocene Kongdian Formation, the Eocene Shahejie Formation, and the Oligocene Dongying Formation. The three members, which are the primary

oil-bearing strata, are the Third (Ek_3), the Second (Ek_2) and the First (Ek_1) members from the base to top of the Kongdian Formation. These form an upward-fining and then -coarsening trend together with an overall red-black-red change in the colour of the strata. The six sand-sets, Sand-sets ZV, ZIV, ZIII, ZII, ZI, and Z0 from the base to top of the First Member, are composed of gray, maroon siltstones and fine-grained sandstones intercalated with maroon, mauve, and gray-green mudstones (Ye et al., 2013). The 17 intervals include Intervals ZV-7 to ZV-1 in Sand-set ZV, and Intervals ZIV-10 to ZIV-1 in Sand-set ZIV.

Previous studies of the heavy minerals and detrital clastic composition of sandstones revealed a southwest-oriented sediment supply that built lacustrine deltas in the Zilaitun Oilfield area (Zhong et al., 2012; Zhang et al., 2013). However, the sedimentary facies associations and their distribution in the deltas remains poorly constrained, and this has hindered exploration and production efforts to produce the abundant hydrocarbons contained within these strata.

3. Datasets and Methods

In the study area, there are 191 wells and 9 cores with a cumulative thickness of 186 m. Wireline log data used in the study include gamma (GR), spontaneous potential (SP), true formation resistivity (RT), sonic travel time (AC), and density (Den). The study area is entirely covered by 3D seismic data, characterized by an effective frequency band between 8 to 60 Hz, a peak frequency of 30 Hz, a vertical seismic resolution of 25-35 m, and signal-to-noise ratio between 1 to 3.5 seconds (two-way travel time) in the interval containing the Kongdian Formation. This study focuses on two issues: identification of lithological assemblages, and seismic geomorphological analysis.

To address the issue of identifying lithological assemblages, emphasis was placed on lithologic composition, sedimentary structures, and depositional cycles (i.e., upward-fining and upward-coarsening cycles) from core and wireline log motifs. In particular, trough cross laminated sandstones and lag gravels were used to identify distributary channels; the dominant sedimentary facies were searched in representative wells; and the colour of mudstone and claystone was used to estimate relative water depth, all of which are critical to determine shallow-water lacustrine delta

deposits (Zou et al., 2008; Girard et al., 2012; Zhu et al., 2017).

Seismic geomorphological analysis was undertaken in six main steps: (1) petrophysical analysis; (2) producing synthetic seismograms; (3) picking of time-equivalent seismic reflections; (4) generation of stratal slices; (5) seismic attribute extraction; and, (6) characterizing seismic geomorphology. The workflow was as follows:

(1) Acoustic impedance, an essential petrophysical parameter for seismic-lithological inversion (Huuse and Feary, 2005; Shi et al., 2012), is the product of density and seismic P-wave (sonic) velocity. Seismic geomorphological analysis requires substantial acoustic impedance contrast between different lithologies (Zhao et al., 2011; Zeng et al., 2012; Zhao et al., 2014).

(2) Synthetic seismograms were generated to tie together seismic and well log data.

(3) Unconformities were systematically picked and traced throughout the study area and define the stratigraphic framework. Moreover, parallel unconformities were used as time-equivalent seismic reflections to generate stratal slices (Zeng et al., 1998a; 1998b; 2013; Zeng and Hentz, 2004).

(4) Stratal slices were generated by proportional interpolation of time-thickness (i.e. proportional isochron maps) in the target intervals between time-equivalent seismic reflections, which allowed for the complex changes in thickness (e.g. those caused by syn-rift faults) (Zeng et al., 1998a; 1998b; Zeng and Hentz, 2004; Zhao et al., 2011).

(5) Root mean square amplitude attribute (RMSAA), a commonly used seismic attribute in seismic geomorphological analysis (Posamentier and Kolla, 2003; Zeng et al., 2007; Chopra and Marfurt, 2008; Zeng et al., 2012), was extracted within each seismic stratal unit, resulting in a successive series of RMSAA maps (See Supplementary Material).

(6) After calibrating to well log data, the seismic geomorphology was delineated in the RMSAA maps. These maps were the basis for determining the sedimentary evolution, and measuring the width and connectivity of sand bodies in the studied succession.

4. Results

4.1. Lithological assemblages

4.1.1. Core representation of lithological assemblages

Within Ek_1, four sandy lithological assemblages, LA1 to LA4, were identified based on core observation, as well as two muddy lithological assemblages, LA5 and LA6 (Table 2).

LA1 is composed of approximately 5-cm-thick lag deposits (Figs. 3A, B, C), gray trough cross-laminated fine-grained sandstones (Figs. 3D, E, F), and green-gray ripple-laminated siltstones from base to top, which constitute an upward-fining cycle from 3–6 m thick. The lag deposits are key to identifying the facies, and contain detrital gravels and mudclasts ranging from 0.5–1.5 cm in diameter. A high-amplitude cylindrical- to bell-shaped wireline log motif characterizes the association (Fig. 2).

LA2 consists of gray-green siltstone and a few fine-grained sandstones, forming an upward-fining cycle from 2–4 m thick. Compared with LA1, this assemblage is thinner and finer-grained, lacking a scour base and lag deposits. The wireline logging motif is serrate, Christmas tree-shaped (Fig. 2).

LA3 is less than 3 m thick, and occurs blow LA2, and displays an upward-coarsening cycle that is mainly composed of gray ripple cross-laminated siltstone. The wireline log motif is funnel-shaped.

LA4 is less than 2.5 m thick, and mainly consist of gray or brown ripple-laminated siltstone intercalated by mudstone, don't displaying clear depositional cycle. A finger- to egg-shaped wireline log motif is typical.

LA5 and LA6 range from 0.5–3 m thick, and consist of brown, maroon or gray-green horizontal-laminated or massive mudstones interbedded with a few thin siltstones (Fig. 3G). Both of them are manifest as smooth or serrated wireline log motifs. LF5 generally overlies LA1 and LA2, whereas LA6 is generally embedded with LA4.

LA1–6 were interpreted to represent large-scale distributary channel, small-scale distributary channel, mouth bar, beach bar, interdistributary bay and shallow lake sedimentary facies in a lacustrine depositional setting (see Table 2), which is discussed further after the seismic geomorphological analysis (see Section 5.1).

4.1.2. Lithological assemblages in the representative well

Wireline log data in the representative well Li16 were used to further examine the lithological assemblages observed in core (Fig. 4). In Sand-sets ZV and ZIV, there are 9 sets of LA1 demarcated by much thicker fine-grained sandstone and cylindrical- to bell-shaped logging motifs, and 14 sets of LA2 marked by thin siltstone to fine-grained sandstone and Christmas tree-shaped log motifs. Either LA1 or LA2 combine with LF5 to form upward-fining depositional cycles. In contrast, there are 7 sets of LF3 marked by thin siltstone and funnel-shaped log motifs.

The thickness of individual sandstone beds was counted and 62% of them are less than 3 m thick, corresponding to mostly LA2, and subordinately LA3 to LA4. Another 22% are 3–6 m thick, corresponding to LA1 to LA2. Finally, 16% of sandstone beds range from 6–10 m thick, corresponding to amalgamated LA1 and (or) LA2 (Fig. 4B).

4.2. Seismic geomorphological analysis

4.2.1. Petrophysical analysis

Acoustic impedance contrasts are marked in Ek_1 strata. As shown in Fig. 5, whether saturated with water, oil or an oil–water mixture, sandstone is of higher acoustic impedance (8,000–10500 kg/m^2·s) than mudstone (5000–8000 kg/m^2·s). Figure 5 displays results from the representative well Li16, considering that acoustic impedance changes with burial depth of the target strata in different wells. However, analogous results were also observed in other wells.

4.2.2. Picking time-equivalent seismic reflectors

Stratal sub-divisions were calibrated between seismic sections and wells by using synthetic seismograms (Fig. 6). The Kongdian Formation is confined between the T3-T45 horizons, shows parallel continuous moderate-amplitude reflections, and local shingled progradational architecture in the western part of the study area (Figs. 7A, B). The seismic horizons T45, T44 and T43 represent the bases of Sand-sets ZV, ZIV and ZIII, respectively, and occur as parallel unconformities marked by onlap and downlap terminations, Therefore, the horizons play time-equivalent seismic reflections, and Sand-sets ZV and ZIV form two 3rd-order stratigraphic sequences, which are bound above and below

by the unconformities (cf. Vail, 1992).

Six stratal slices were interpolated between T44-T45 and nine between T43-T44 in proportion to the time thickness of ZV7-ZV1 and ZIV10-ZV1 intervals, respectively (Fig. 7C). As a result, seven and ten seismic stratal units vertically spaced at 12-25 ms (two-way travel time) with an approximate thickness of 15-35 m were generated.

The T42, T41 and T3 horizons correspond to the bases of Sand-sets ZII and ZI, and the Shahejie Formation, respectively, forming unconformities marked by onlap and truncation reflection terminations. This is evidence of extreme stratal denudation with a thickness ranging between 50–250 m. As such, the T42, T41 and T3 horizons are not time-equivalent seismic reflections (Zeng et al., 1998a; 1998b).

4.2.3. Characterizing seismic geomorphology

4.2.3.1. Types of seismic geomorphology

Seventeen RMSAA maps were derived from seismic attribute extraction. Calibrating to core and wireline logs from representative wells (Figs. 8-10) shows that high RMSAA coincides with sandstone-prone zones, although a quantitative correlation between RMSAA values and net sandstone thickness was not obtained. Three types of seismic geomorphology in zones of moderate to high RMSAA were found to match to the sandy lithological assemblages: (1) ribbon-shaped geomorphology that range from 62-500 m wide and slightly sinuous, coinciding with LA1 or LA2. All of the delineated RMSAA maps show that the ribbon-shaped geomorphology extends and increasingly bifurcate towards the southwest; (2) disk-like geomorphology with an area of less than 1 km^2 occurring at the termination of LA1 or LA2, and coinciding with LA3; and, (3) insular elliptic or lunate-shaped geomorphology that is mostly less than 0.5 km^2 in area, sits in the front of or lateral to LA1 or LA2, and coincides with LA4.

In addition to the different types of geomorphology represented by high RMSAA zones, two kinds of seismic geomorphology in zones of low RMSAA were found to match to the muddy lithological assemblages: (1) spotted geomorphology occur between neighboring ribbon-shaped geomorphologies, shown by moderate-RMSAA spots scattered in low-RMSAA zone and coinciding

with LA5; (2) flat geomorphology across widespread low-RMSAA zones, coinciding with LA6.

4.2.3.2. Plan-view patterns in seismic geomorphology

The ribbon-shaped geomorphologies show distributive and anastomosing patterns in plan-view on RMSAA maps. The distributive pattern is characterized by a lower density of ribbon-shaped geomorphologies than the anastomosing pattern, and typically occurs in the ZV-6, ZV-5, ZV-4 and ZIV-2 intervals (Figs. 8B', C', D', 10D'). The anastomosing pattern more commonly present in the ZV-3, ZV-2, ZV-1, ZIV-10, ZIV-5 and ZIV-4 intervals (Figs. 9A', B', C', D', 10A', B').

4.2.3.3. Sedimentary evolution

According to the distribution of high RMSAA representing sandy deposits, three phases of sedimentary evolution are clearly demarcated in the ZV7 to ZV1 and ZIV10 to ZIV1 intervals: progradation, aggradation, and retrogradation.

A retrogradational phase is especially prevalent in the ZV-7 to ZV-4 interval, and is characterized by the ribbon-shaped geomorphology that overall decreases in density and extension distance into the paleo-lake (Fig. 8). This distributive ribbon-shaped geomorphology is typical of retrogradation.

A progradational phase is best imaged in the ZV-4 to ZV-1 interval, and is manifest by the ribbon-shaped geomorphology that overall increases in density and distance of lakeward extension (Figs. 8D', 9A'-C'). This is matched by a shift towards ribbon-shaped geomorphology from distributive to anastomosing pattern.

An aggradational phase is displayed in the ZIV-5 and ZIV-4 intervals, and is illustrated by a consistent density of the ribbon-shaped geomorphology with an anastomosing pattern (Figs. 10A' and B'). However, an aggradational phase was not interpreted for the ZV-1 and ZIV-10 interval due to the presence of parallel unconformities -- T44-- between the two intervals, despite the anastomosing pattern and consistent density of the ribbon-shaped morphology (Figs. 9C' and D').

A retrogradational phase still occurs as the ribbon-shaped geomorphologies that decrease in overall quantity and lakeward extension distance up-section through the ZIV-4 to ZIV-2 interval (Figs. 10B', C' and D'). This is matched by a change from anastomosing to distributive patterns.

Sand-set V displays retrogradation and then progradation, whereas Sand-set VI shows the complete sedimentary evolution including aggradation, retrogradation and progradation (Table 3).

4.2.3.4. Sand body architecture

The average width of the ribbon-shaped geomorphology (representing the main sand body) in each interval of the ZV and ZIV Sand-set was surveyed from the delineated RMSAA maps, whereas the average thickness of sand bodies was determined from wells (Table 3). The bifurcating distribution of the ribbon-shaped geomorphology was taken to be indicative of sand body connectivity. The results show that the distributive pattern consists of narrower, thicker, and more poorly-connected sand bodies than the anastomosing pattern. There is a negative correlation between average width and average thickness of the sand bodies (Fig. 11).

5. Discussion

5.1. Shallow-water lacustrine deltas in Ek_1 strata

Based on sedimentological characteristics, the six lithological assemblages correspond directly to specific sedimentary facies and environments (Table 2): (1) LA1 has the coarsest grain size, and forms upward-fining cycles with a scoured base and lag deposits, and is therefore interpreted as large-scale distributary channel facies; (2) LA2 has slightly finer grain size, forms upward-fining cycles and is interpreted as small-scale distributary channel facies; (3) LA3 shows upward-coarsening cycles, sits below LA2, and is thus interpreted as mouth bar facies; (4) LA4 is characterized by the finest grain size and ripple lamination, and is embedded in LA6 (shallow lake facies), and is thus interpreted as beach bar facies; (5) LA5 always overlies LA1 or LA2, and is thus interpreted as interdistributary bay facies; and, (6) LA6 is the mud-richest assemblage, and represents shallow lake facies. Each of the facies represent a distinct sub-environment within a lacustrine delta.

In addition to facies analysis, three other observations support the interpretation of shallow-water lacustrine deltas in Ek_1. First, mudstone from Ek_1 is generally mottled and grey-green to maroon colour, indicating a weakly-oxidized shallow water environment into which the channels flowed. Second, both

core analysis and interpretations of wireline logs reveal that the dominant sedimentary facies are distributary channels rather than mouth bars, which is an important distinguishing feature of shallow-water lacustrine deltas (Zou et al, 2008; Zhu et al., 2008; Li et al., 2009; Zhao et al., 2011; Girard et al., 2012; Wang et al., 2012; Jin et al., 2014; Zhu et al., 2017). Third, widespread, continuous, parallel moderate-amplitude reflectors and local shingled progradational reflection architecture are typical of shallow-water lacustrine delta stratigraphy (Zhao et al., 2011; Jin et al., 2014).

5.2. Comparation to modern shallow-water lacustrine deltas

Based on knowledge of the sedimentary facies, a link between the three types of seismic geomorphology in zones of moderate to high RMSAA and the sedimentary facies were built. The ribbon-shaped, disk-like, insular elliptic or lunate-shaped geomorphology correspond distributary channel, mouth bar, and beach bar facies, respectively. Therefore, the RMSAA maps show widespread distributary channel facies indicative of shallow-water lacustrine deltas, and the distributive and anastomosing patterns represent two contrasting styles of distributary channel complex.

Modern sedimentary systems are in some ways analogous to the sedimentary facies derived from the seismic geomorphological analysis in this study. The Ganjiang Delta, for example, is a modern shallow-water lacustrine delta that is located where the Ganjiang River spills into Poyang Lake in southeastern China (Zou et al., 2008; Duan et al., 2014; Jin et al., 2014) (Fig. 12A). Poyang Lake covers an area of 4,627 km^2 during flood season, but only 146 km^2 in the dry season due to more than 10 m of lake-level fluctuation. The Ganjiang Delta has an area of 1,544 km^2 and formed on the western gentle slope (at 0.1° gradient) of Poyang Lake. In the northeastern portion of the outer deltaic plain, distributary channels are 30–500 m wide and are 10–40 km long (Fig. 12B) (Duan et al., 2014). Distributary channels mostly form an anastomosing pattern, but two distinctive distributive patterns also occur. The mouth bar is composed of radial sand bars with a total area of 2 km^2 (Fig. 12D). The Ganjiang delta front deposits consist of fine-grained sandstone, siltstone, and mudstone. Moreover, a beach bar with an approximate area of 6 km^2 is isolated within the central part of the lake (Fig. 12C). It is clear that the deltas revealed by seismic geomorphological analysis in the Zilaitun Oilfield are comparable in the width of distributary channels, the area of the mouth bar, as well as the sediment

composition of the Ganjiang Delta.

5.3. Effectiveness of seismic geomorphology for mapping shallow-water lacustrine deltas

Seismic data has long been used to investigate the sedimentary facies that comprise thick strata based on seismic reflection configurations and architecture, using so called "seismic stratigraphy" (Van Wagoner et al., 1988; Vail, 1992). In contrast, seismic geomorphological analysis provides additional detail about the size and orientation of sedimentary facies, being advantageous for seismic stratigraphic analysis. However, it remains poorly constrained if seismic data are not of a high enough resolution to map sedimentary facies distribution patterns, despite seismic geomorphological analyses being undertaken from a variety of different sedimentary environments. Zeng et al. (2012) proposed that various clastic sedimentary facies are commonly characterized by far larger horizontal dimensions than vertical dimensions, and are thus detectable on seismic attribute maps, and carried out a case study from the Qingshankou Formation in Qijia Area, Songliao Basin, northeastern China. They used stratal slices at 4 ms sampling spacing, and produced a few seismic amplitude attribute maps that clearly imaged shallow-water lacustrine deltas.

In this study, acoustic impedance contrasts, resulting in large reflection coefficients and ultimately seismic amplitudes, occur in different lithologies. To a large extent, amplitude attribute maps are analogous to sandstone isopach maps or sandstone percentage maps. Seismic geomorphological analysis revealed results that strongly indicate a shallow-water lacustrine delta origin for the strata, including: (1) seismic geomorphology closely match sedimentary facies recognized in core and wireline log data; (2) RMSAA maps show that distributary channels extend and bifurcate increasingly towards the southwest, indicating a southwest-prograding delta, and thus, southwest-orientated sediment supply (Zhong et al., 2012; Zhang et al., 2013); (3) supporting the findings of previous studies of modern and ancient shallow-water lacustrine deltas (Overeem et al., 2003; Geleynse et al., 2011; Girard et al., 2012; Zhu et al., 2017), distributive and anastomosing channel patterns are clearly imaged in the RMSAA maps; (4) the phases of sedimentary evolution from retrogradation to progradation occurring in Sand-set V, and aggradation to retrogradation, and then to progradation occurring in Sand-set VI coincide with those in 3rd-order sequences (c.f.,

Posamentier et al, 1988; Vail, 1992); (5) seismic geomorphological results are analogous to modern sediment distribution patterns in the Ganjiang Delta. Based on the weight of evidence, we propose that seismic geomorphological analysis is highly effective for mapping shallow-water lacustrine delta deposits.

5.4. Lake-level change controls on stratigraphic evolution and channel sand body architecture

Stratigraphic evolution is controlled by tectonic subsidence, climate, sediment supply and base-level (i.e., lake-level in lacustrine basins) change, forming progradational, aggradational, and retrogradation stratal stacking patterns (Posamentier et al., 1988; Vail, 1992; Zhao et al., 2011). In the study area, the parallel unconformities T45, T44 and T43, as well as the overall consistent lithologic assemblages indicate stable tectonic subsidence and sediment supply in the development of Sand-sets ZV and ZIV. In contrast, the angle disconformities T41, T3 and T0, which bound strata that thin toward the central Zilaitun area, indicate differential basement subsidence due to active tectonics (Figs.1C, 7A, B). Previous studies of spore-pollen assemblages reveal that the Bohai Basin was characterized by a constant dry, cool subtropical climate during development of the First Member of Kongdian Formation (Liu et al., 2012). Under such conditions, only lake level change would have been responsible for delta evolution. Therefore, delta evolution can be used to decipher lake-level changes.

Even small lake-level change results in lacustrine basins greatly expanding and shrinking in settings with gentle slope such as Poyang Lake. This is why it is commonly proposed to control channel-generated sand body architecture (Lou, 1999; Hoy and Ridgway, 2003; Overeem et al., 2003; Olariu and Bhattacharya, 2006; Zou et al, 2008; Zhu et al., 2008; Li et al., 2009; Wang et al., 2012). In this study, lake-level fall is typically indicated by deltaic progradation in Intervals ZV-4, ZV-3, ZV-2 and ZV-1 (Fig. 9). At the same time, deltas distributary channels transformed from distributive patterns to anastomosing patterns, and the channel sand bodies became thinner, wider, and more well-connected (Table 3). This indicated that lake-level fall accelerated lateral migration and bifurcation of the channels. By contrast, lake-level rise is indicated by deltaic retrogradation in Intervals ZV-7, ZV-6 ZV-5 and ZV4 (Fig. 8), while channel sand bodies became thicker, narrower, and less well-connected (Table 3). This indicated that lake-level rise accelerated vertical accretion and restrained bifurcation of the channels. Resultantly, lake-level change caused the negative correlation between average width and average thickness channel sand bodies.

6. Conclusions

Using core, seismic, and wireline log data, seismic geomorphological analysis was used to map lacustrine deltas in the First Member of the Kongdian Formation, in the Zilaitun Oilfield. The major findings of the analysis include:

(1) Four sandy sedimentary facies - large-scale distributary channels, small-scale distributary channels, mouth bars, and beach bars - were identified, as well as muddy interdistributary bay and shallow lacustrine facies. The dominance of distributary channel facies, together with mottled grey-green to maroon mudstones and local shingled progradational seismic architecture, suggests a shallow-water lacustrine delta origin for the strata.

(2) Seismic geomorphological analysis clearly differentiates sandy sedimentary facies from muddy facies. Sandy distributary channels have either distributive or anastomosing patterns in plan-view. Progradation of the delta is indicated by an upward shift from distributive to anastomosing patterns. Aggradation is manifest as a consistent anastomosing pattern. Retrogradation is indicated by an upward shift from anastomosing to distributive patterns. These results are comparable to what is observed from modern deltas.

(3) Distributive patterns tend to yield thicker, narrower, and less connected sand bodies than anastomosing patterns. This, as well as a negative correlation between average width and average thickness of distributary channel sand bodies, is attributed to lake-level change.

The study shows the benefit of such a high-resolution seismic geomorphologic analysis in terms of constraining channel sand body dimensions, orientations and plan-view geometries. This fills a gap in the literature, as few previous studies have undertaken this type of work (e.g., Zeng et al., 2012; Zhu et al., 2013). The results provide generic insight into the depositional evolution and stratigraphic architecture of lacustrine depositional systems, including insight into variability in sandstone connectivity, which has global significance.

Acknowledgements

We thank the finance support of National Science and Technology Major Project of China (No. 2016ZX05026-003). We are grateful for constructive and positive suggestions from reviewer Howard D. Johnson that helped improve the quality of the manuscript.

References

Allen, M.B., Macdonald, D.I.M., Zhao, X., Vincent, S.J., Brouet-Menzies, C., 1997. Early Cenozoic two-phase extension and late Cenozoic thermal subsidence and inversion of the Bohai Basin, Northern China. Marine and Petroleum Geology, 14, 951-972.

Carter, D.C., 2003. 3-D seismic geomorphology: Insights into fluvial reservoir deposition and performance, Widuri field, Java Sea. AAPG Bulletin, 87(6), 909-934.

Chopra, S., Marfurt, K.J., 2008. Emerging and future trends in seismic attributes. The Leading Edge, 27(3), 298-318.

Davies, R.J., Posamentier, H.W., Wood, L.J., 2006. Seismic geomorphology: applications to hydrocarbon exploration and production. Geological Society, London. Special Publication, 277, 1-274.

Donaldson, A.C., 1974. Pennsylvanian sedimentation of central Appalachians. Special Papers. Geological Society of America, 148, 47-48.

Dong, Y.L., Zhu, X.M., Xian, B.Z., Cheng, K.N., Wang, P., 2014. Mapping sediment-dispersal characteristics using seismic geomorphology: Late Paleogene to Neogene, Qinan Sag, Huanghua Depression, China. Marine and Petroleum Geology, 54, 180-197.

Duan, D.P., Hou, J.G., Liu, Y.M., Wang, C.G., Gao, J., 2014, Quantitative research of fluvial-dominated delta front sedimentary system: a case study of Poyang Lake delta. Acta Geologica Sinica, 32(2), 270-277 (In Chinese with English abstract).

Feng, Y.L., Li, S.T., Lu, Y.C., 2013. Sequence stratigraphy and architectural variability in Late Eocene lacustrine strata of the Dongying Depression, Bohai Bay Basin, Eastern China. Sedimentary Geology, 295, 1-26.

Geleynse, N., Storms, J.E.A., Walstra, D.J.R., Jagers, H.R.A., Wang, Z.B., Stive, M.J.F., 2011. Controls on river delta formation: insights from numerical modeling. Earth and Planetary Science

Letters, 302(1), 217-226.

Gilbert, G.K., 1985. The topographic features of lake shores. U S geological survey, 5th annual report (1883-1884). Washington. Unite States Government Printing Office, 69-123.

Girard, F., Ghienne, J.-F., Rubino, J.-L., 2012, Channelized sandstone bodies ('cordons') in the Tassili N'Ajjer (Algeria & Libya): snapshots of a Late Ordovician proglacial outwash plain. Geological Society London Special Publications, 368(1):355-379.

Hubbard, S.M., Smith, D.G., Nielsen, H., 2011. Seismic geomorphology and sedimentology of a tidally influenced river deposit, Lower Cretaceous Athabasca oil sands, Alberta, Canada. AAPG Bulletin, 95(7), 1123-1145.

Huuse, M., Feary, D.A., 2005. Seismic inversion for acoustic impedance and porosity of Cenozoic cool-water carbonates on the upper continental slope of the Great Australian Bight. Marine Geology, 215, 123-134.

Jin, Z.K, Li, Y., Gao, B.S., Song, B.Q., He, Y.H., Shi, L., Li, G.Z., 2014. Depositional model of modern gentle-slope delta: A case study from Ganjiang Delta in Poyang Lake. Acta Sedimentologica Sinica, 32(4), 710-723 (In Chinese with English abstract).

Kolla, V., Bourges, P., Urruty, J.M., Safa, P., 2001. Evolution of deep-water Tertiary sinuous channels offshore Angola (west Africa) and implications for reservoir architecture. AAPG Bulletin, 85, 1373-1405.

Li, Y.H., Liu, C.Y., Du, Y.G., Wang, X.J., Huang, J.X., 2009. Sedimentary characteristics of shallow water delta and lake shoreline control on sand bodies of Chang 8 oil-bearing interval of the upper Triassic Yanchang Formation in northwest Ordos Basin. Journal of Palaeogeography, 11(3), 265-274 (In Chinese with English abstract).

Liu, S.L., Wang, Q.F., Gong, Y.J., Zhang, R.X, Feng, Z.P., Yang, N., Tong, O., 2012. Paleogene microfossil assemblages from the Bohai area and their importance for the oil and gas exploration. Jouranl of Stratigraphy, 36(4), 700-709 (In Chinese with English abstract).

Loucks, R.G., Moore, B.T., Zeng, H.L., 2011. On-shelf lower Miocene Oakville sediment-dispersal patterns within a three-dimensional sequence-stratigraphic architectural framework and implications for deep-water reservoirs in the central coastal area of Texas. AAPG Bulletin, 95(10),

1795-1817.

Miall, A.D., 1985. Architectural-element analysis: a new method of facies analysis applied to fluvial deposits. Earth Science Review, 22(2), 261-308.

Miall, A.D., 2002. Architecture and sequence stratigraphy of Pleistocene fluvial systems in the Malay Basin, based on seismic time-slice analysis. AAPG Bulletin, 86, 1201-1216.

Olariu, C., Bhattacharya, J.P., 2006. Terminal distributary channels and delta front architecture of river-dominated delta systems. Journal of Sedimentary Research, 76, 212-233.

Overeem, I., Kroonenberg, S.B., Veldkamp, A., Groenesteijn, K., Rusakov, G.V., Svitoch, A.A., 2003. Small-scale stratigraphy in a large ramp delta: recent and Holocene, sedimentation in the Volga delta, Caspian Sea. Sedimentary Geology, 159(3), 133-157.

Posamentier, H.W., Jervey, M.T., Vail, P.R., 1988. Eustatic controls on clastic deposition I: conceptual framework. In: Wilgus, C.K., Hastings, B.S., Kendall, C.G.S.C., Posamentier, H.W., Ross, C.A., Van Wagoner, J.C. (Eds.). Sea Level Changes: An Integrated Approach. SEPM Special Publication, 42, 110-124.

Posamentier, H.W., Kolla, V., 2003. Seismic geomorphology and stratigraphy of depositional elements in deep-water settings. Journal of Sedimentary Research, 73(3), 367-388.

Posamentier, H.W., 2002. Ancient shelf ridges: A potentially significant component of the transgressive systems tract: Case study from offshore northwest Java. AAPG Bulletin, 86(1), 75-106.

Ren, J., Tamakib, K., Li, S., Zhang, J., 2002. Late Mesozoic and Cenozoic rifting and its dynamic setting in Eastern China and adjacent areas. Tectonophysics, 344(3-4), 175-205.

Shi, W.Z., Zhao, Z.K., Jiang, T., Miao, H.B., Wang, X.L., 2012. Identifying updip pinch-out sandstone in nearshore subaqueous fans using acoustic impedance and the instantaneous phase in the Liangjia area, Yitong Basin, China. Marine and Petroleum Geology, 30, 32-42.

Sylvester, Z, Deptuck, M.E., Prather, B.E., Pirmez, C., O'Byrne, C., 2012. Application of the principles of seismic geomorphology to continental-slope and base-of-slope systems: case studies from seafloor and near-seafloor analogues. SEPM Special Publication, 99, 31-59.

Vail, P.R., 1992. The evolution of seismic stratigraphy and the global sea-level curve. In: Dott R H Jr.

(ed.), Eustasy: The historical ups and downs of a major geological concept. Geological Society of America Memoir, 180, 83–91.

Van Wagoner, J.C., Posamentier, H.W., Mitchum, R.M., Vail, P.R., Sarg, J.F., Loutit, T.S., Hardenbol, J., 1988. An overview of sequence stratigraphy and key definitions. In Sea Level Changes–An Integrated Approach C.K. Wilgus, B.S. Hastings, C.G. St. C. Kendall, H.W. Posamentier, C.A. Ross and J.C. Van Wagoner, Eds.), 39–45. SEPM Special Publication, 42.

Wang, J.H., Chen, H.H., Jiang, T., Tang, Z.X., Zhao, B.F., Xu, D.H., 2012. Sandbodies frameworks of subaqueous distributary channel in shallow-water delta, Xinli area of Songliao Basin. Earth Science, 37(3), 556-564 (In Chinese with English abstract).

Wood, L.J., Kristine, L., 2009. Quantitative seismic geomorphology of a Quaternary levee-channel system, offshore eastern Trinidad and Tobago, northeastern South America. AAPG Bulletin, 93(1), 101-125.

Ye, L., Zhang, J.X., Lu, G.C., 2013. Paleogene structure-stratigraphic framework and multiple episode evolution in Kongnan Area, Huanghua Depression. Earth Science, 38(2), 379-389 (In Chinese with English abstract).

Zeng, H.L., Backus, M.M., Barrow, K.T., Tyler, N., 1998a. Stratal slicing, part I: Realistic 3-D seismic model. Geophysics, 63(2), 502-513.

Zeng, H.L., Henry, S.C., Riola, J.P., 1998b. Stratal slicing, part II: Real seismic data. Geophysics, 63(2), 514-522.

Zeng, H.L., Hentz, T.F., 2004. High-frequency sequence stratigraphy from seismic sedimentology: Applied to Miocene, Vermilion Block 50, Tiger Shoal Area, offshore Louisiana. AAPG Bulletin, 88(2), 153-174.

Zeng, H.L., Loucks, R.G., Brown, L.F., 2007. Mapping sediment dispersal patterns and associated systems tracts in fourth and fifth order sequences using seismic sedimentology: Example from Corpus Christi Bay, Texas. AAPG Bulletin, 91(7), 981-1003.

Zeng, H.L., Zhu, X.M., Zhu, R.K., Zhang, Q.S., 2012. Guidelines for seismic sedimentologic study in non-marine postrift basins. Petroleum Exploration and Development, 39(3), 275-284.

Zeng, H.L., Zhu, X.M., Zhu, R.K., 2013. New insights into seismic stratigraphy of shallow-water

progradational sequences: subseismic clinoforms. Interpretation, 1(1), 35-51.

Zhang, S.J., Pu, X.G., Li, Y., Yan, Z.K., Qian, G., Qiu, D.Z., Xiao, D.Q., Liu, Z.C., Yuan, S.Q., 2013. Provenance Analysis of ZaoIII Reservoir Group in Southern Kongdian of Huanghua Depression. Geoscience, 27(1), 186-190 (In Chinese with English abstract).

Zhao, D.N., Zhu, X.M., Dong, Y.L., Wu, D., Zhu, M., 2014. Application of seismic sedimentology to prediction of beach and bar sandbodies in gentle slope of lacustrine basin: A case study of the Lower Cretaceous in Chepaizi area, Junggar Basin, NW China. Petroleum Exploration and Development, 41(1), 60-67.

Zhao, W.Z., Zou, C.N., Chi, Y.L., Zeng, H.L., 2011. Sequence stratigraphy, seismic sedimentology, and lithostratigraphic plays: Upper Cretaceous, Sifangtuozi area, southwest Songliao Basin, China. AAPG Bulletin, 95(2), 241-265.

Zhong, W., Pu, X.G., He, Y.B., Chen, C.W., Lin, C.M., Han, W.Z., Zhang, W., Wu, C., 2012. Provenance of the Member 2 of Paleogene Kongdian Formation in Kongnan area, Huanghua Depression, Bohai Bay Basin. Journal of Palaeogeography, 14(6), 707-718 (In Chinese with English abstract).

Zhu, W.L., Li, J.P., Zhou, X.H., Guo, Y.H., 2008. Neogene shallow water deltaic system and large hydrocarbon accumulations in BohaiBay, China. Acta Sedimentologica Sinica, 26(4), 575-582 (In Chinese with English abstract).

Zhu, X.M., Zeng, H.L., Li, S.L, Dong, Y.L., Zhu, S.F., Zhao, D.N., Huang, W., 2017. Sedimentary characteristics and seismic geomorphologic responses of a shallow-water delta in the Qingshankou Formation from the Songliao Basin, China. Marine and Petroleum Geology, 79, 131-148

Zou, C.N., Zhao, W.Z., Zhang, X.Y., Luo, P., Wang, L., Liu, L.H., Xue, S.H., Yuan, X.J., Zhu, R.K., Tao, S.Z., 2008. Formation and Distribution of shallow-water deltas and central-basin sandbodies in large open depression lake basins. Acta Geologica Sinica, 82(6), 813-825 (In Chinese with English abstract).

Fig. 1. Regional tectonic location (A, B) and structural patterns (C, after Ye et al., 2013) of the Zilaitun Oilfield, Huanghua Depression, Bohai Bay Basin, Eastern China. 1- Tectonic belt; 2- Normal fault in plan-view; 3- Secondary depocenter area; 4- Anticline; 5- Well site; 6- City or town; 7- Normal fault. *Nm*- the Neogene Minghuazhen Formation; *Ng*- the Neogene Guantao Formation; *Ed*- the Oligocene Dongying Formation; Es_1, Es_3- the First and Third Member of the Eocene Shahejie Formation, respectively; $Ek_1^{Z0\text{-}III}$, $Ek_1^{ZIV\text{-}V}$ - Sand-sets Z0 to ZIII and ZIV to ZV of the First Member of the Paleocene Kongdian Formation, respectively; Ek_2, Ek_3- the Second and the Third Member of the Paleocene Kongdian Formation, respectively; *Mz*- the Mesozoic; *C*- the Carboniferous; *O*- the Ordovician.

Fig. 2. Lithological assemblages and interpretation of sedimentary facies from 1650–1694 m in Well Z9. Colors in the lithologic column represent the primary sediment colors. Three lithological assemblages, LA1, LA2 and LA5, were identified. LA1 is the most coarse-grained, has a scoured base, contains lag deposits, and fines upwards. It is interpreted as large-scale distributary channel (LDC) facies. LA2 is finer-grained, fines upwards, and was interpreted small-scale distributary channel facies (SDC); LA5 has a muddy composition, overlies LA1 or LA2, and is interpreted as interdistributary bay deposits (IDB). See Fig. 1B for the location of Well Z9.

Fig. 3. Core photos showing the lithology and sedimentary structures comprising the lithologic assemblages LA1 (A-F) and LA5 (G). A, B, C- lag deposits at 1674.06 m, 1679.17 m, and 1680.76 m in Well Z9, respectively. D, E, F- gray fine-grained sandstones with trough cross lamination at 2100.11 m, 2104.72 m and 2104.94 m deep in Well Z19-12, respectively. Laminae were partly drawn on the photos to demonstrate trough cross lamination. G- maroon massive mudstones from 1650.68–1652.58 m in Well Z9. See Fig. 1B for the locations of Wells Z19-12 and Z9.

Fig. 4. Lithological assemblages and interpretation of sedimentary facies (A), and distribution frequency histogram of sandstone thickness (B) in Sand-sets ZV-ZIV from the representative Well Li16. The colors in the lithologic column represent lithologic colors. Lithological assemblages LA1,

LA2 and LA3 are distinguished in compositions, depositional cycles and the resulted wireline log motifs. Note that distributary channel facies rather than mouth bar facies are dominant. See Fig. 1B for the location of Well Li16. LDC- Large-scale distributary channel; SDC- Small-scale distributary channel; MB- Mouth bar; IDB- Interdistributary bay; SH- Shoal; SL- Shallow lake.

Fig. 5. Cross plot of natural gamma (GR) against acoustic impedance in the First Member of the Kongdian Formation in Well Li16. Sandstone is of higher acoustic impedance than either mudstone or claystone. See Fig. 1B for the Well Li16 location.

Fig. 6. Synthetic seismogram made to tie seismic to Well Li16. Sand-set ZV and ZIV were identified to lie between horizons of T45-T44 and T44-T43. T45, T44 and T43 play as the bases of Sand-sets ZV, ZIV and ZIII, respectively. 6 and 9 stratal slices along the tops of Intervals ZV7-ZV2 and ZIV10-ZIV2 in Well Li16 one to one were prepared to interpolate.

Fig. 7. Interpretation of seismic horizons and stratigraphic architecture in two representative seismic sections (A and B), and the positions of the stratal slices (C). As the bases of Sand-sets ZV, ZIV and ZIII, respectively, the horizons T45, T44 and T43 present parallel unconformities marked by downlap and toplap reflection terminations. As the bases of Sand-sets ZII and ZI, and the Shahejie Formation, respectively, the horizons T42, T41 and T3 present angular unconformities marked by onlap and truncation reflection terminations. Between T43-T44 and T44-T45, 6 and 9 stratal slices were interpolated in proportion to time thickness of Intervals ZV7-ZV1 and ZIV10-ZIV1 in Well Li16, respectively. As a result, the stratal slices together with the horizons of T45, T44 and T43 confine 7 and 10 seismic stratal units. See Fig. 1B for the seismic sections' locations.

Fig. 8. Seismic geomorphological maps (A', B', C', D') redrawn from the delineated RMSAA maps (A, B, C, D) in Intervals ZV-7, ZV-6, ZV-5 and ZV-4, respectively. Well data were utilized to calibrate the relationship between RMSAA (i.e. seismic geomorphologies) and lithological assemblages (LA1 to LA6). See Well Z15 for other wells' heads. Sedimentary retrogradation is illustrated by

ribbon-shaped geomorphologies overall decreasing in quantity and the lake-ward extension distance, which is matched by a distributive pattern. RMSAA- root means square amplitude attribute.

Fig. 9. Seismic geomorphological maps (A', B', C', D') redrawn from the delineated RMSAA maps (A, B, C, D) in Intervals ZV-3, ZV-2, ZV-1 and ZIV-10, respectively. Well data were utilized to calibrate the relationship between RMSAA (i.e. seismic geomorphologies) lithological assemblages (LA1 to LA6). See Well Z15 for other well locations. From Interval ZV-3 to ZV-1, progradation is illustrated by ribbon-shaped geomorphology increasing overall in density and distance of lakeward extension, matched by an anastomosing pattern. RMSAA- root means square amplitude attribute.

Fig. 10. Seismic geomorphological maps (A', B', C', D') redrawn from the delineated RMSAA maps (A, B, C, D) in Intervals ZIV-5 to ZIV-2. Well data were utilized to calibrate the relationship between RMSAA (i.e. seismic geomorphology) and lithological assemblages (LA1 to LA6). A progradation phase is illustrated by ribbon-shaped geomorphology that decreases in density and basinward extension from Interval ZIV-4 to ZIV-2, along with a shift from the anastomosing to distributive pattern. The seismic geomorphological distribution in Interval ZIV-5 is similar to that in Interval ZIV-4, indicating an aggradation phase along with an anastomosing pattern. RMSAA- root means square amplitude attribute.

Fig. 11. Cross plot of average width against average thickness of ribbon-shaped sand bodies in each interval of Sand-sets ZV-ZIV, showing a negative correlation. Average width and average thickness data are from Table 3.

Fig. 12. Geographic location of Ganjiang Delta (A, adapted after Jin et al., 2014) and aerial photographs showing sedimentary facies (B, C, D. from Google Earth).

Table 1. The Paleogene stratigraphic division in the Zilaitun Oilfield, Huanghua Depression, Bohai Bay Basin, China.

Table 2. Characteristic summary of sandy lithological assemblages and interpretation of sedimentary facies based on core and the tied well data.

Table 3. Statistical average width and average thickness of ribbon-shaped sand bodies in each interval of Sand-sets ZV-ZIV. Width data were measured from the ribbon-shaped seismic geomorphologies such as those in Figs. 8, 9, 10. Average thickness data were counted from lithological assemblages LA1 and LA2 in wells.

Figure1

Click here to download high resolution image

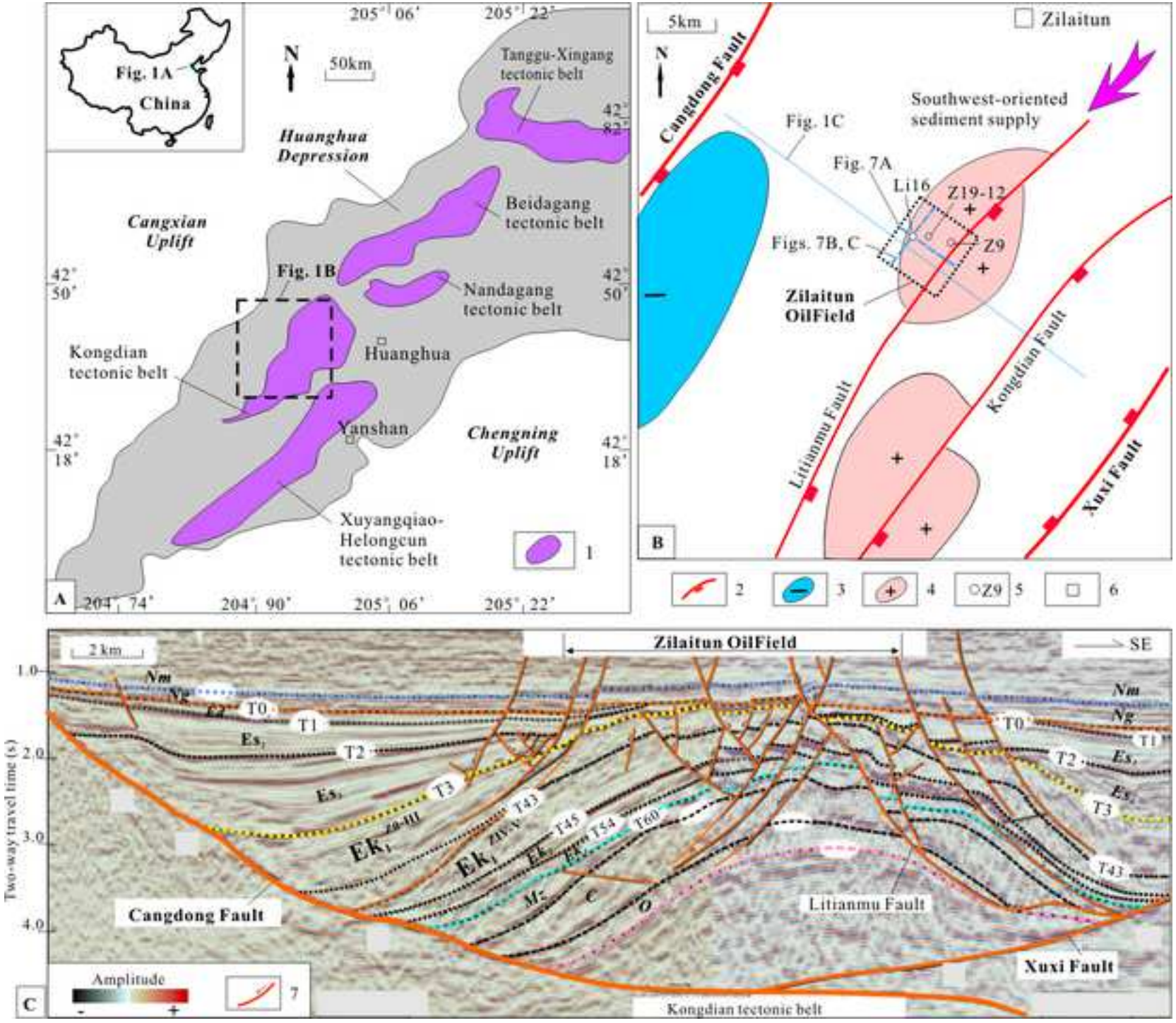

Figure2

Click here to download high resolution image

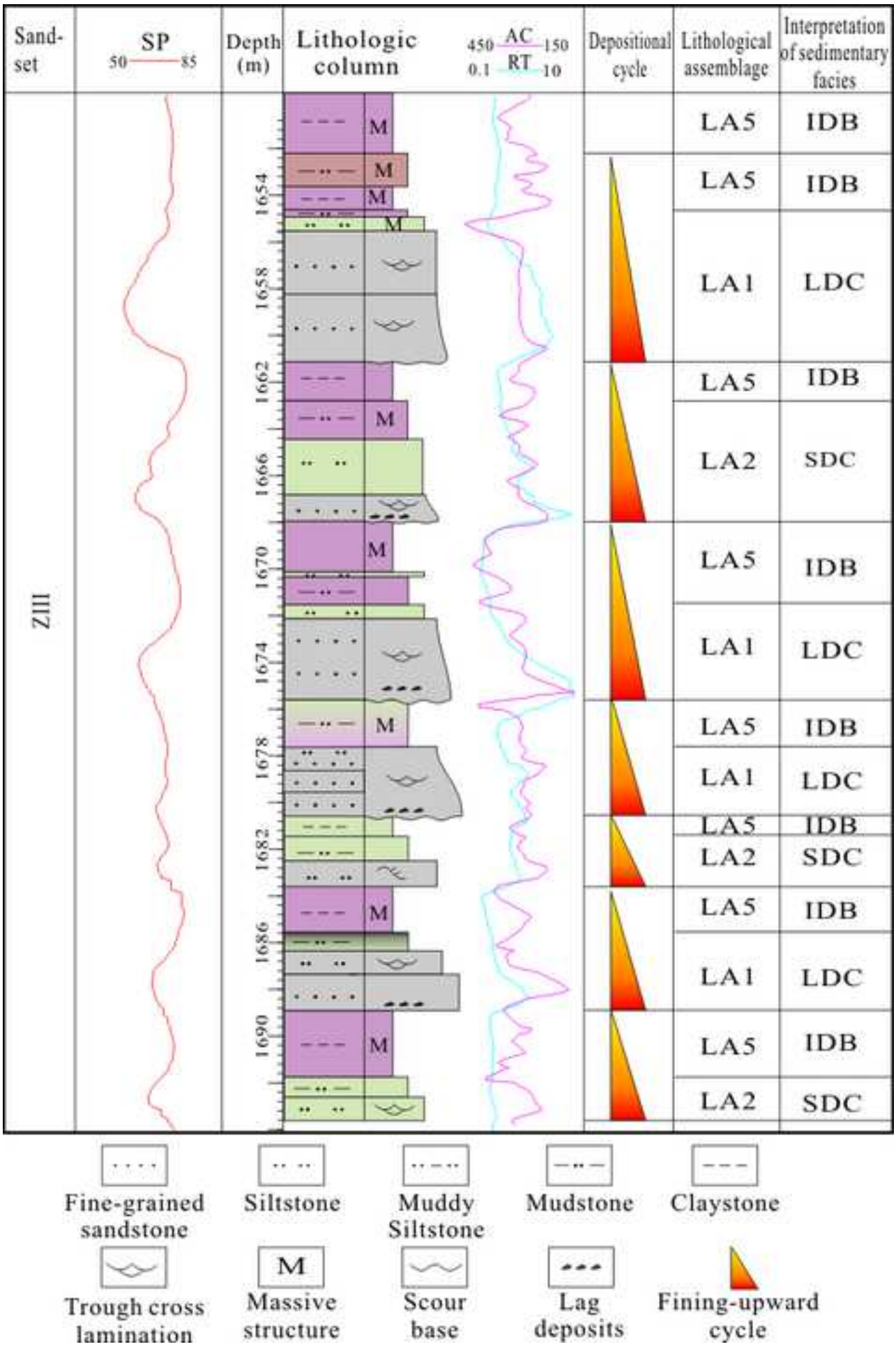

Figure3

Click here to download high resolution image

Figure4

Click here to download high resolution image

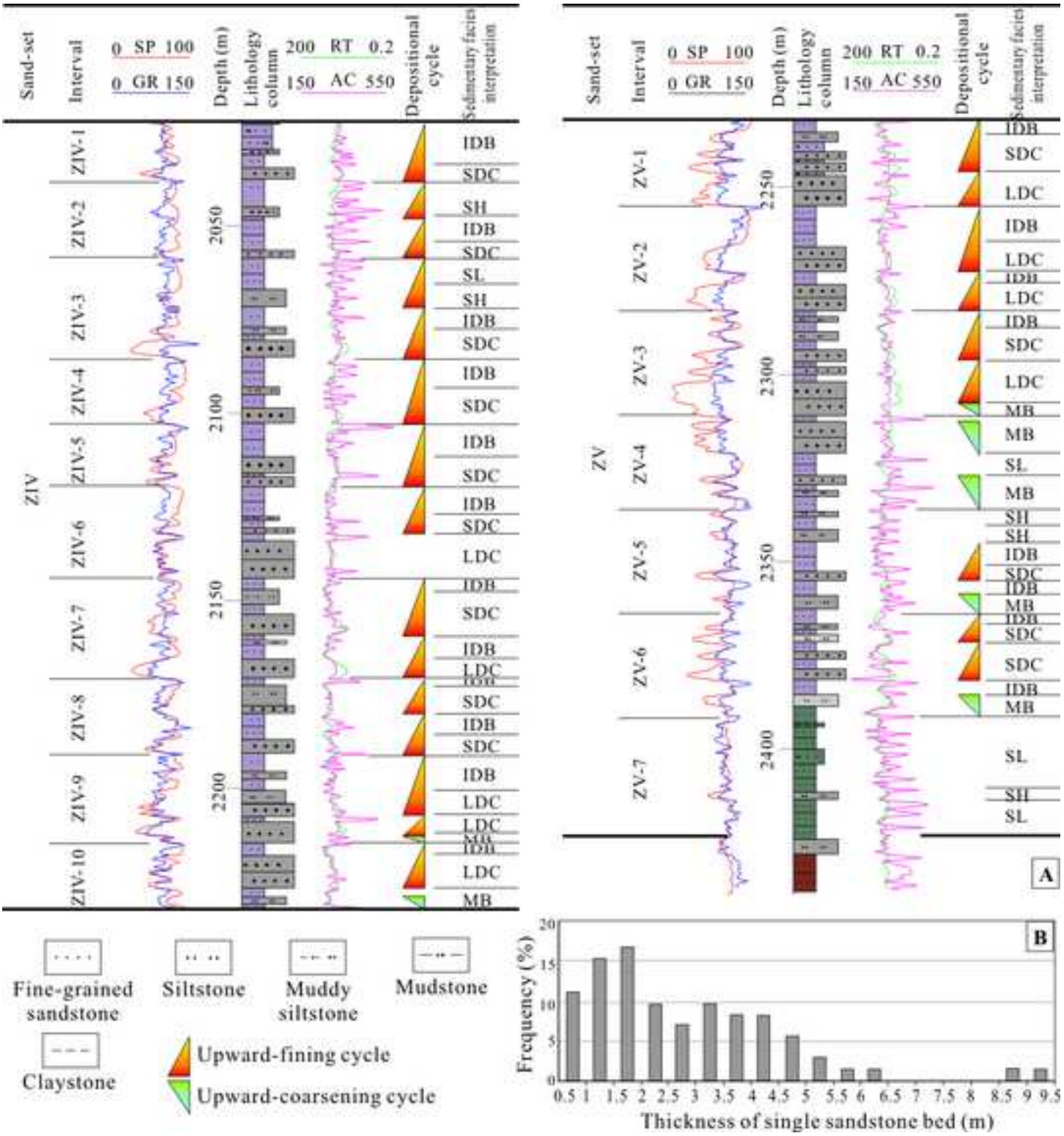

Figure5

Click here to download high resolution image

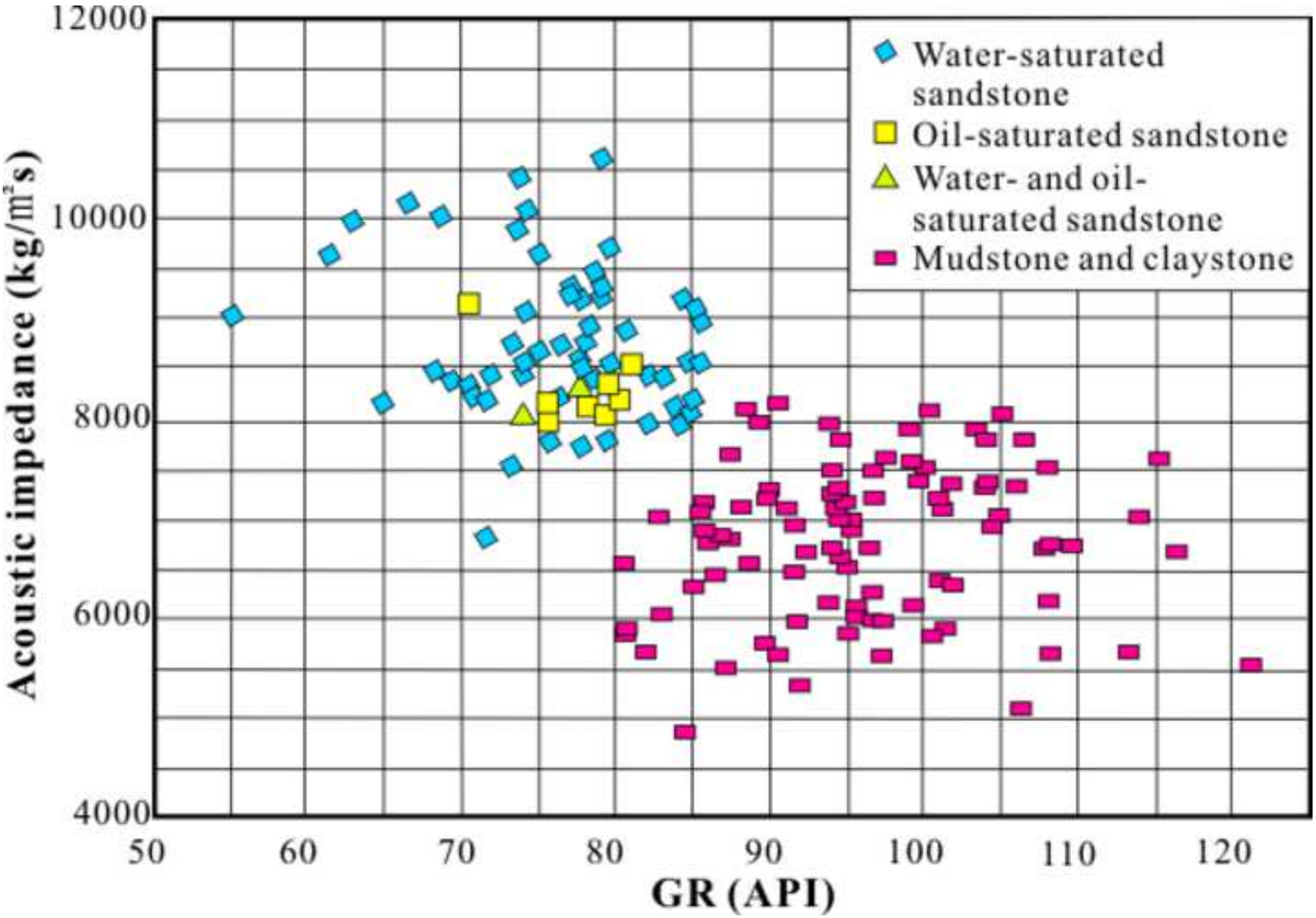

Figure6

Click here to download high resolution image

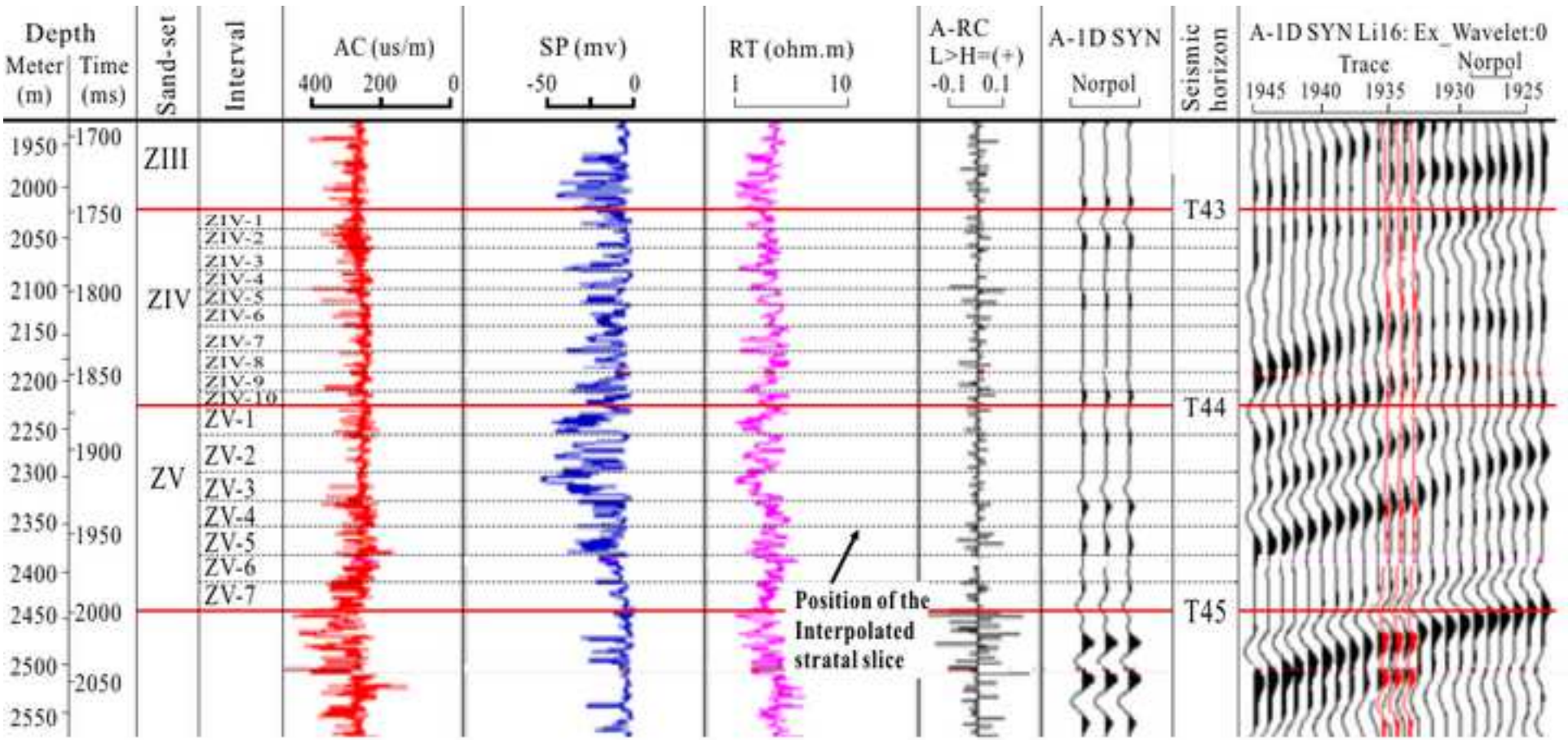

Figure7

Click here to download high resolution image

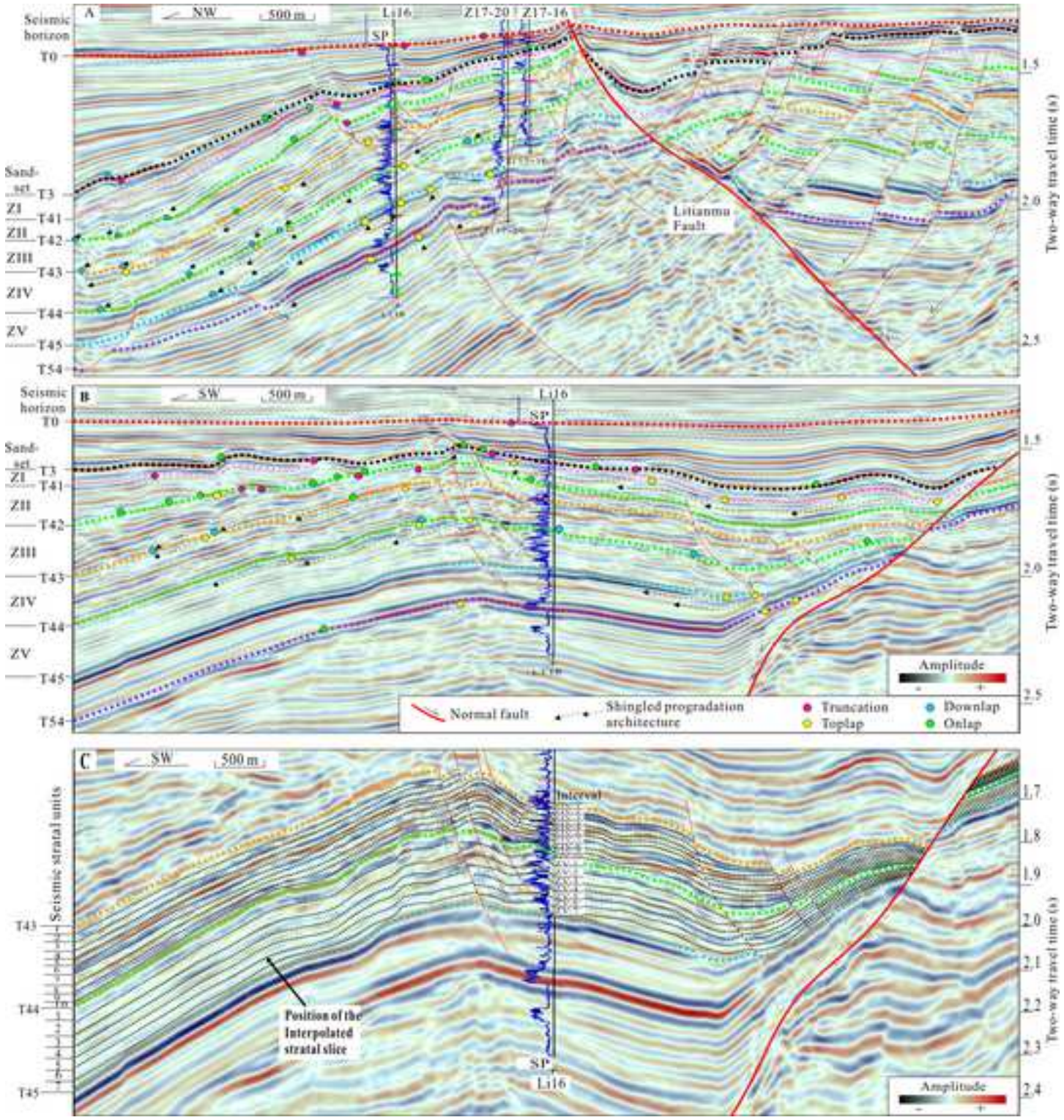

Figure8

Click here to download high resolution image

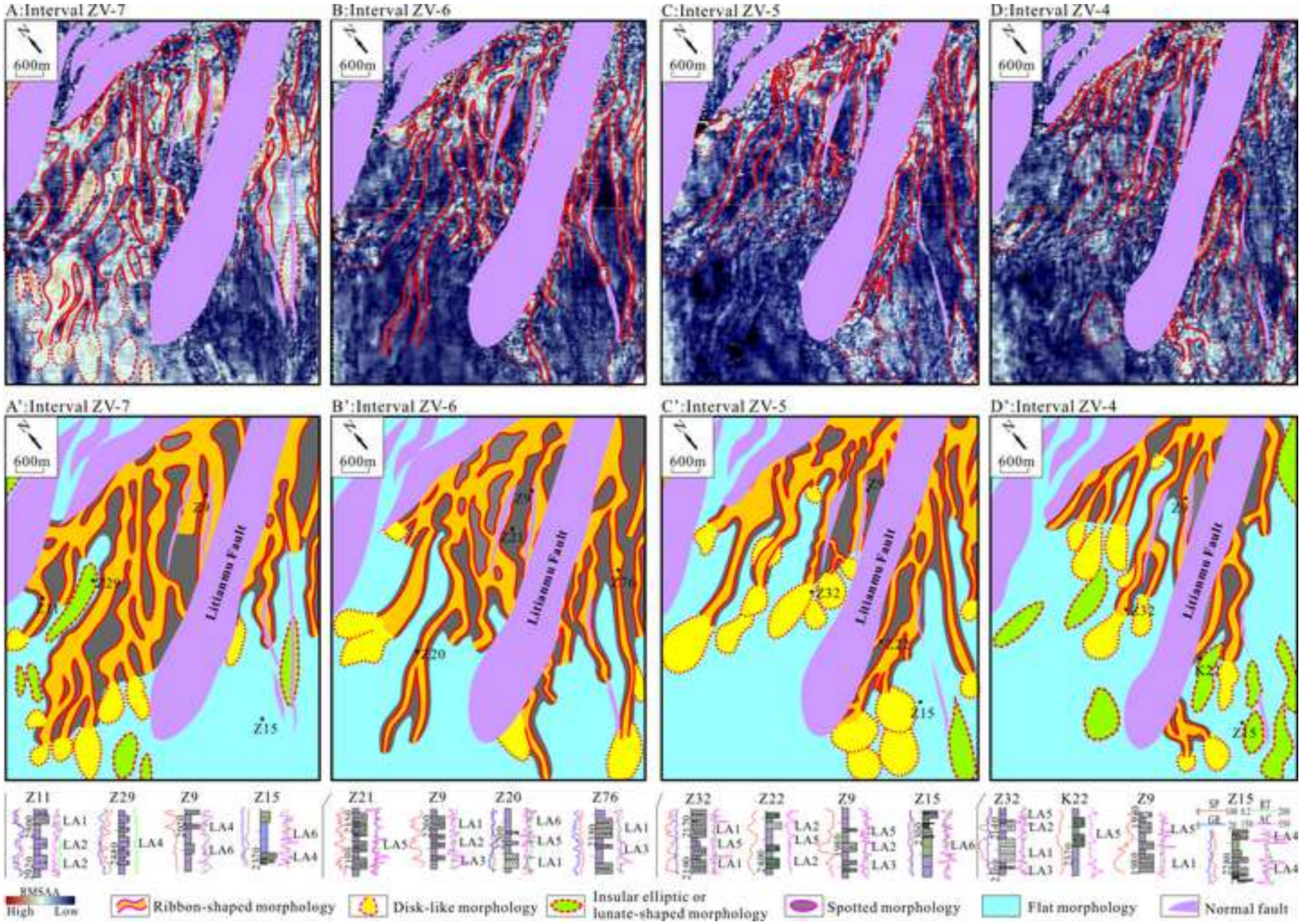

Figure9

Click here to download high resolution image

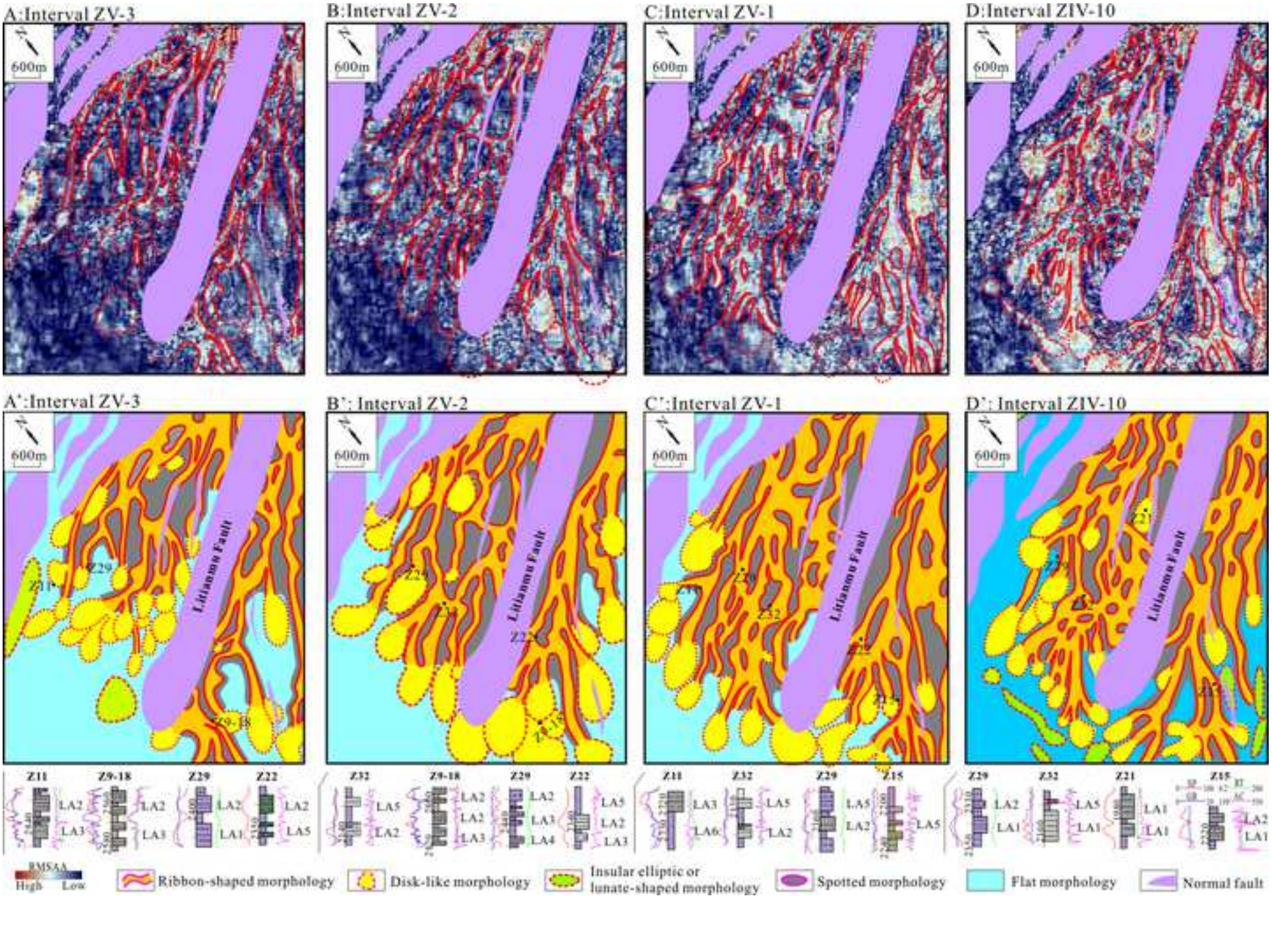

Figure10

Click here to download high resolution image

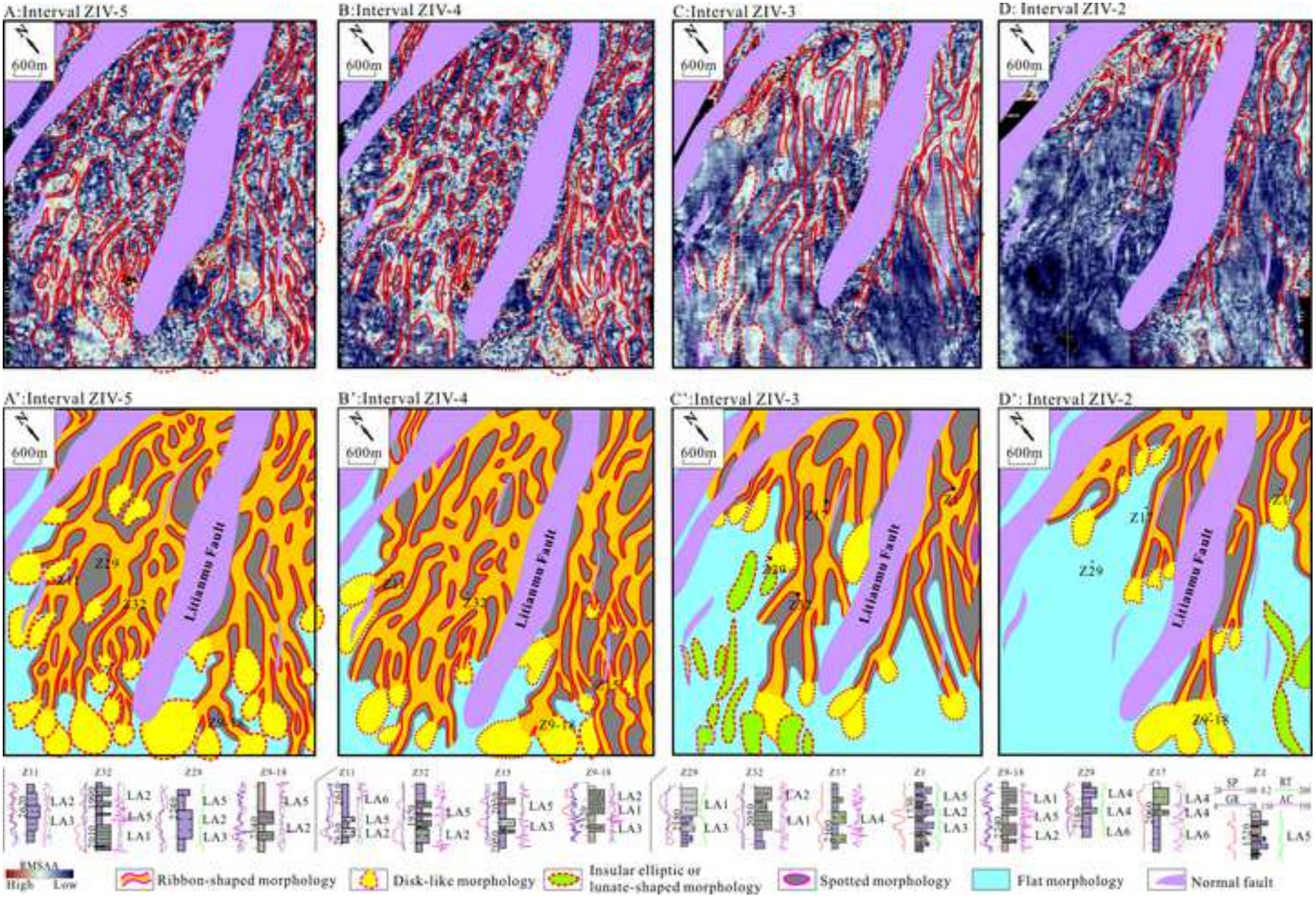

Figure11

Click here to download high resolution image

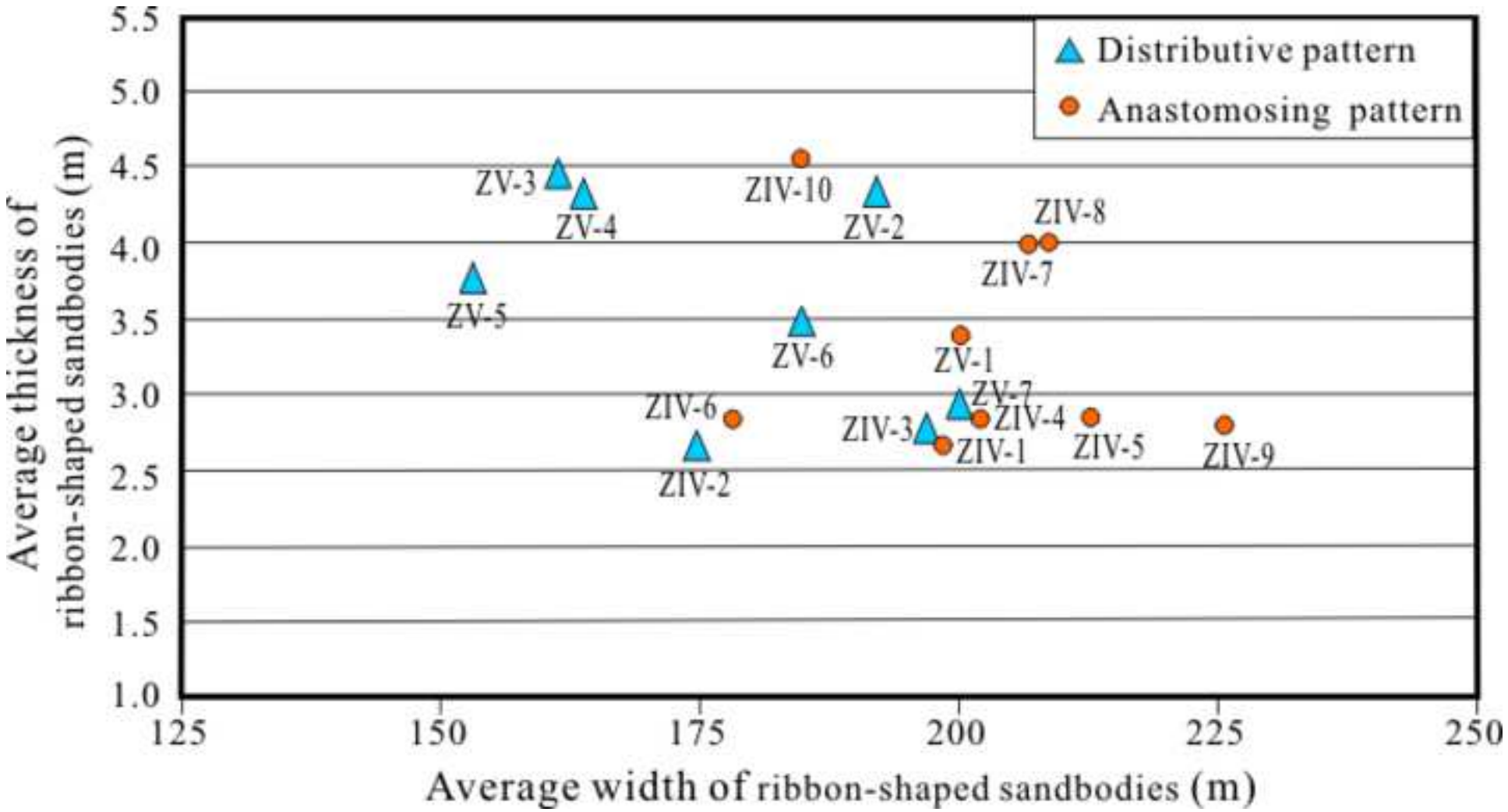

Figure12

Click here to download high resolution image

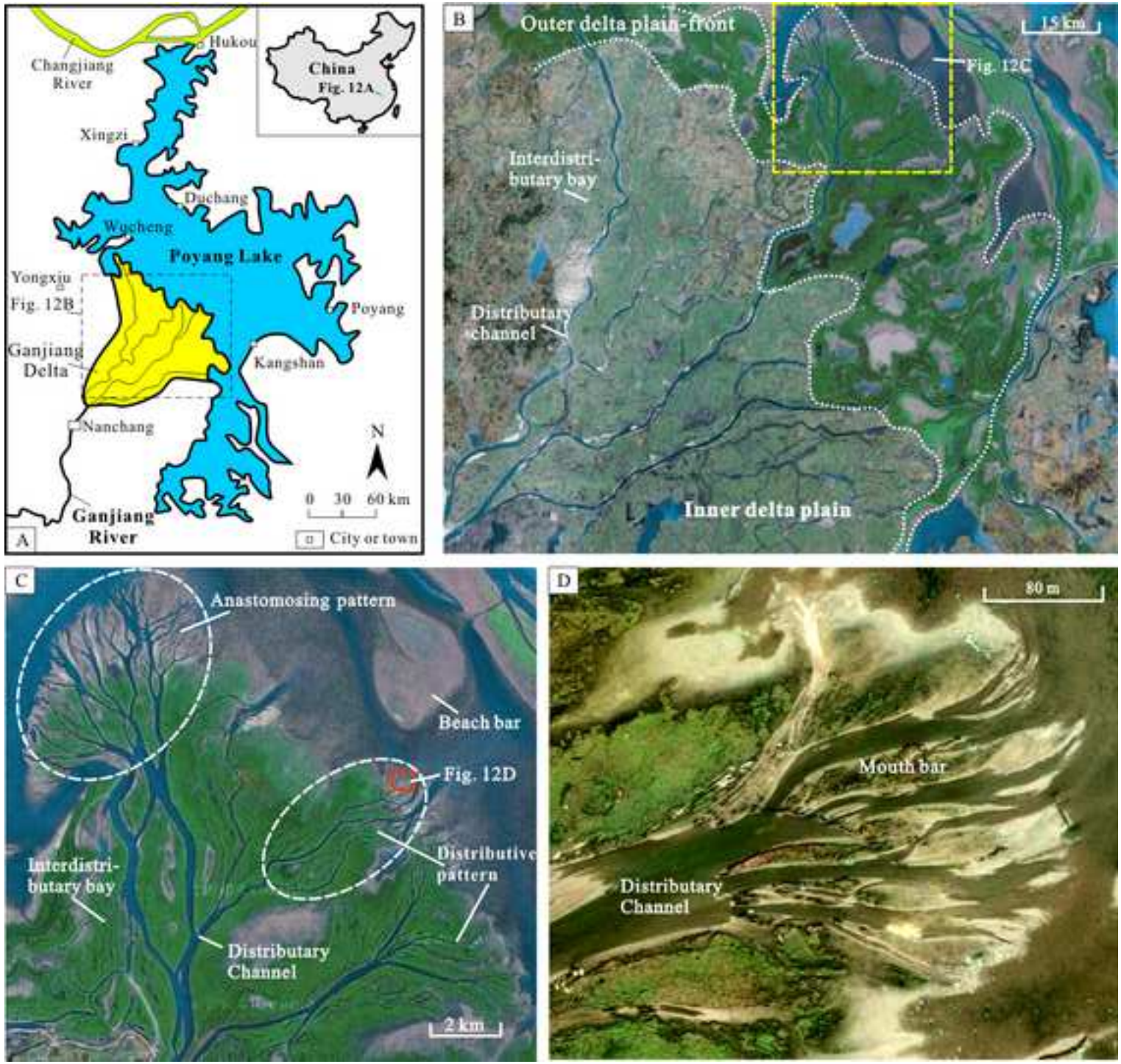

Table1

Click here to download high resolution image

System	Series	Formation	Member	Sand-set	Interval	Seismic horizon
Neogene		Guantao				To
Paleogene	Oligocene	Dongying				T1
	Eocene	Shahejie				T3
	Paleocene	Kongdian	First	Z0		T40
				ZI		T41
				ZII		T42
				ZIII		T43
				ZIV	ZIV-10 to ZIV-1	T44
				ZV	ZV-7 to ZV-1	T45
			Second			T54
			Third			T60

Table2

Click here to download high resolution image

Types of lithologic assemblage	Lithological composition	Sedimentary structure	Depositional cycle	Thickness	Log motif	Interpretation of sedimentary facies
LA1	Gray fine-grained sandstones, green-gray siltstones and muddy siltstones	Scoured base, lag deposit, Trough cross-lamination	Fining-upwards; bottom lag deposits	3 to 6 m	High-amplitude cylindrical- to bell-shaped	Large-scale distributary channel
LA2	Gray-green muddy siltstones, siltstones and a few fine-grained sandstones	Trough cross-lamination	Fining-upwards	2 to 4 m	Serrate, Christmas tree-shaped	Small-scale distributary channel
LA3	Thin muddy siltstones and siltstones	Wave cross-lamination	Coarsening-Upwards	Less than 3 m	Funnel-shaped	Mouth bar
LA4	Gray, brown muddy siltstones and siltstones intercalated by thin mudstones	Cripple lamination, wave cross-lamination	Loss of lag deposits and grain-size change trend	Less than 2.5 m	Finger- to egg-shaped	Beach bar

Table3

Click here to download high resolution image

Sand-group	Interval	Ribbon-shaped sandbodies							Sedimentary evolution
		Amount	Width (m)			Average thickness (m)	Average width to thickness (0 40 80 120)	Distributary pattern	
			Minimum	Maximum	Average				
ZIV	ZIV-1	31	108	385	199	2.6	77	Anastomosing	Progradation
	ZIV-2	17	92	369	175	2.7	65	Distributive	
	ZIV-3	20	92	446	197	2.8	70	Distributive	Retrogradation
	ZIV-4	30	77	369	202	2.8	72	Anastomosing	
	ZIV-5	31	100	446	213	2.9	73	Anastomosing	
	ZIV-6	29	62	385	178	2.8	64	Anastomosing	
	ZIV-7	25	62	423	207	4.0	52	Anastomosing	Aggradation
	ZIV-8	30	62	438	209	4.0	52	Anastomosing	
	ZIV-9	26	77	500	226	2.8	81	Anastomosing	
	ZIV-10	29	69	354	185	4.6	40	Anastomosing	
ZV	ZV-1	26	92	500	200	3.4	59	Anastomosing	Progradation
	ZV-2	17	108	292	192	4.4	44	Distributive	
	ZV-3	17	85	462	162	4.5	36	Distributive	
	ZV-4	12	77	223	164	4.3	38	Distributive	
	ZV-5	13	62	223	153	3.8	40	Distributive	
	ZV-6	15	85	308	185	3.5	53	Distributive	Retrogradation
	ZV-7	18	123	346	200	2.9	69	Distributive	